Physica D 56 (1992) 84–106
North-Holland

PHYSICA D

Theory of reentrant excitation in a ring of cardiac tissue

Hiroyuki Ito[1] and Leon Glass

Department of Physiology, McGill University, 3655 Drummond Street, Montreal, Quebec, Canada H3G 1Y6

Received 12 July 1991
Revised manuscript received 10 December 1991
Accepted 17 December 1991
Communicated by J. Guckenheimer

A cardiac pathology, reentrant tachycardia, is caused by the sustained circulation of activation along a reentrant path in cardiac tissue. A new theoretical model for wave propagation in discrete excitable media employing coupled maps with continuous time is used to derive analytical stability criteria for the uni-directional circulation of the excitation pulse on the ring of cardiac tissue. Numerical simulations of the model that incorporate experimentally measurable characteristics of the cardiac tissue reproduce the experimental data quantitatively. The complex oscillations in the cycle length of unstable tachycardia observed experimentally are quasiperiodic oscillations that arise via the multiple Hopf bifurcation in high dimensional maps.

1. Introduction

Since the beginning of this century, many irregular rhythms of excitation have been identified both experimentally and clinically in cardiac physiology [1–4]. Recent development of nonlinear mathematics enables us to understand some of these classical phenomena (for reviews of recent studies, see refs. [5, 6]). For example, periodic stimulation of excitable cardiac systems gives phase locking and chaotic rhythms, which can be predicted by low dimensional maps [7, 8]. The complex rhythms in the conduction of excitation in excitable cardiac tissue [9] and through the atrio-ventricular (AV) node [10–12] have been studied also by using low dimensional maps. These applications of low dimensional dynamical systems succeed because the dynamics is well described by a small number of variables with simple evolution rules. However, there are phenomena in which high dimensionality seems to be essential. For example, the turbulent excitation waves of ventricular fibrillation appear to defy description using low dimensional dynamical systems [13–16]. In this paper, we analyze the dynamics of reentrant excitation in a one dimensional ring of cardiac tissue and show that in this problem high dimensional maps give a reasonable approximation to the observed dynamics.

In the normal heart, the rhythm is set by specialized cardiac tissue, the cardiac pacemaker, that periodically discharges starting a wave of excitation that spreads throughout the cardiac muscle. The period of the heartbeat in such a case is set by the ionic properties of the membrane currents that constitute the cardiac pacemaker. However, in some pathologies, there can be reentrant paths of excitation in which the excitation travels in a "circus" movement [17, 18]. In such a case, the period of the reentrant circulation, if it persists, is set by the conducting properties of the cardiac tissue. During this reentrant excitation, the period of the cardiac rhythm is usually faster than normal and the resulting

[1]Present address: Department of Information Science and Communication, Kyoto Sangyo University, Kamigamo, Kita-ku, Kyoto 603, Japan.

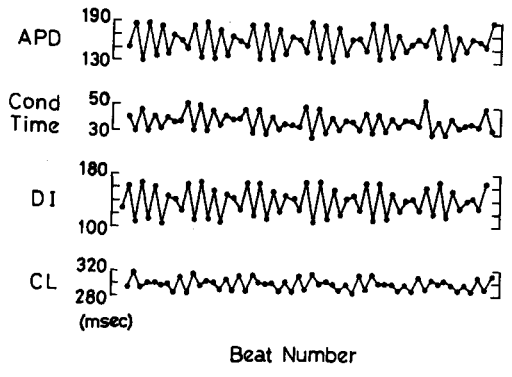

Fig. 1. Spontaneous oscillations accompanied by reentrant excitation in a ring of cardiac tissue (taken from ref. [19]). Activation was detected at a single site in the ring by intracellular recording. Oscillations of action potential duration (APD); conduction time; diastolic interval (DI); and cycle length (CL) are shown for 56 cycles of circulation of excitation in the ring. Each quantity is plotted as a function of beat number and the time scales in the ordinates are identical except for the conduction time, which is increased twofold. The diastolic interval is the same as the recovery time. For the definition of each quantity and more detailed information, see section 2 and section 6 where we reproduce these data using our theoretical model.

rhythm is called a *tachycardia*. Reentrant excitation is one of the major mechanisms of cardiac arrhythmias and is believed to be responsible for different arrhythmias such as atrial flutter, AV nodal reentrant tachycardia, and ventricular tachycardia [17].

The recognition of the significance of reentrant excitation in the genesis of cardiac arrhythmias is due largely to researchers early in this century who demonstrated that an annular ring of tissue could support reentrant excitation. Mayer [2] demonstrated such a phenomenon in conducting tissue in jellyfish and Mines [3] observed a similar effect in a ring of atrial tissue from turtle heart. More recently, in a beautiful series of experiments, Frame and Simson [19–21] demonstrated that uni-directional circulation of excitation can be initiated on a piece of ring-shaped atrial tissue dissected from dog heart. By recording the activation at multiple sites in a ring of tissue, they observed that complex irregular oscillations of the length of time needed to circulate around the ring (cycle length) of the excitation (fig. 1) lead to conduction block and spontaneous termination of reentry.

The original theoretical model of reentrant excitation was developed by Wiener and Rosenblueth in 1946 [22]. They considered a ring of length L, where the conduction velocity was v, and the period of circulation is L/v. After the excitation, the cardiac tissue needs a certain time interval called the refractory period θ to recover its ability to conduct excitation. Hence in order to have a stable reentrant excitation, we must have $L/v > \theta$. The Wiener–Rosenblueth model therefore can account for a stable period or an excitation that would block following the first circuit of a ring of tissue; the Wiener–Rosenblueth model cannot account for the complex oscillations in the period of reentrant circulation observed in the Frame and Simson experiment seen in fig. 1.

Subsequent to the Wiener–Rosenblueth model, many theoretical models for the propagation of excitation in excitable tissue have been proposed. These theoretical models are usually posed as nonlinear partial differential equations [23–25] or cellular automata [26–30]. Most of these models are based on the microscopic physical mechanism of generation and propagation of excitation established experimentally. Due to the complexity of the mathematical descriptions (partial differential equations) and the discrete nature of the phase space (cellular automata), analytical studies are difficult and most studies are carried out by computer simulations. By using these models, we can reproduce some of the complex dynamics observed in a macroscopic level of cardiac tissue (reentrant excitation in one-dimensional ring, spiral waves in two-dimensional sheet, etc.). However, because of the complexity of the model, it appears difficult to understand clearly what is the essential mechanism leading to such complex behaviours directly from the microscopic level.

Understanding the mechanisms leading to reentrant tachycardias and ventricular fibrillation is an important medical problem since such arrhythmias are life threatening. From the physio-

logical point of view, the main interest is the question "under which physiological conditions do these arrhythmias occur?". We need a theoretical model that can be used as a powerful tool for both analytical investigation and numerical experiment to explore this problem keeping a connection with both the microscopic level and the macroscopic level of cardiac tissue. Recently we proposed a theoretical model that uses coupled maps and allows analytical studies and efficient numerical computations [31]. We formulated our model based on two important characteristics in a "mesoscopic" level of cardiac tissue: both conduction velocity and the action potential duration (the time during which cardiac tissue is excited) depend on the time elapsed since the passage of the last pulse of excitation in the cardiac tissue. Since these characteristics can be easily measured experimentally, we can examine the change in macroscopic dynamical behaviours under different characteristics and compare our theoretical results directly with the experimental data.

Although the main interest in this paper is the macroscopic dynamical behaviour, the mesoscopic characteristics can be studied separately based on ionic mechanism of cardiac tissue [9, 32, 33]. For example, if we can obtain these characteristics by numerical simulations of complex partial differential equations (e.g., the Beeler–Reuter model [34]), we can use them for further analytical investigation and numerical simulations of the macroscopic dynamics by using our model. Such an approach has been proposed previously by some authors. Krinsky [35] studied a system of two coupled excitable cells and discussed the excitation echo and its stability by using his θ-model. His model also uses coupled maps, but incorporates a different cellular property from our model, the latency of the action potential after the stimulus. Miller and Rinzel [33] studied the instability of periodic wavetrains of impulse in one-dimensional excitable cable of neural tissue. They first computed the dispersion relation (a relation between speed and stimulation frequency) of a single wave by numerical simulation of a partial differential equation (the Hodgkin–Huxley model). Then they reduced the system of many wavetrains into a simple interactive pulse model based on the obtained dispersion relation. However the instability in their study is derived from the non-monotonic dispersion relation that is not the case of cardiac tissue.

In this article, we apply our theoretical model to the problem of reentrant excitation in a one dimensional ring of cardiac tissue. In section 2, we introduce our theoretical model and show that the dynamics of the reentrant excitation on the ring is described by N coupled maps. We derive analytical criteria for the stability of reentrant excitation in section 3. Details of the analytical calculations are presented in the appendices. In section 4, the change in dynamical behaviours with different cellular characteristics are examined using the analytical results given in section 3 and numerical simulations. In sections 2–4, we consider the homogeneous system in which the spacing between the neighbouring excitable elements is identical everywhere. The effect of inhomogeneity on the system is discussed in section 5. The application of these results to reentrant tachycardias is studied in section 6, where we compare the results of numerical simulations with the experimental data by Frame and Simson. We discuss the results in section 7.

2. Model

2.1. Basic model

We assume that the ring of cardiac tissue is composed of some number of independent aggregates of heart cells in which excitation occurs almost simultaneously. We consider the aggregate as the basic excitable element in our theoretical model and call it a *cell*. Thus, the term cell is used in this paper in a technical sense (as in cellular automata), and does not correspond to a single biological cell. We consider a ring of N

excitable elements (cells) with identical properties. Each cell is connected to two neighbouring cells by a conducting cable. The cell can be excited by an incoming pulse from exciting neighbouring cells. When a cell gets excited, the cell stays at the exciting state (*action potential*) for a finite interval which is called *action potential duration* (APD). At the beginning of the action potential, the cell emits an excitation pulse which conducts through the conducting cable. We assume that the conduction time per unit length, τ, is given by

$$\tau = f(T) = \alpha \exp(-T/\beta) + \gamma, \quad \text{if } T \geq \theta, \qquad (1)$$

where α, β and γ are positive parameters and θ is the *refractory time* of the cell. T is the time interval from the end of the last action potential to the beginning of the present action potential at the cell which is emitting the pulses and is called *recovery time*. The recovery time in this system is the same as the diastolic interval which is often used in cardiac physiology. Such a relationship is called the *recovery curve* in cardiac physiology (fig. 2a) and the functional form in eq. (1) is often used for fitting of experimentally measured recovery curves [12]. This curve reflects slow conduction velocity for short recovery times. The excitation pulse propagates to both neighbouring cells with the same conduction velocity.

The APD also depends on the recovery time of the cell. Such a relationship is called the *electrical restitution curve*. In general, APD is a monotonically increasing function of T with a finite asymptote (fig. 2b). We assume a relationship

$$\text{APD} = g(T) = -\delta \exp(-T/\varepsilon) + \zeta, \quad \text{if } T \geq \theta, \qquad (2)$$

where δ, ε, and ζ are positive parameters [9, 32, 36]. After the end of the action potential, the cell must spend a constant duration θ to recover its excitability. If $T < \theta$, the excitation is blocked. The next excitation will be induced by the earliest arriving pulse after the refractory period.

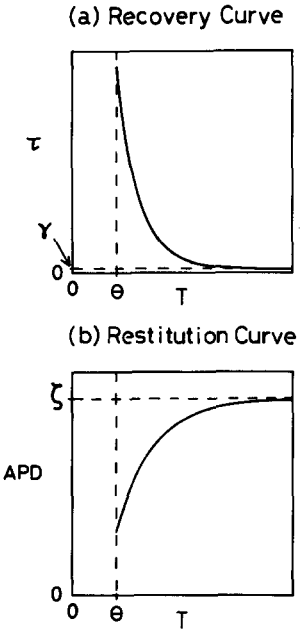

Fig. 2. Two characteristics of cardiac tissue: (a) recovery curve and (b) restitution curve. The conduction time τ is a monotonically decreasing function of the recovery time T with a finite asymptote γ. The APD increases monotonically until a finite asymptote ζ as the recovery time T increases. The excitation cannot occur when T is less than the refractory time θ.

To carry out the numerical simulation, for each cell, one must keep track of the time of the end of the last action potential t_{last} and the time of the beginning of the next action potential t_{next}. The integration proceeds in the following steps. At any time t, the cell with the smallest $t_{\text{next}} > t$ is excited. The time variable t jumps to t_{next}. For each neighbouring cell, the arrival time of the pulse from this cell is calculated by using the distance between the two cells and the conduction time per unit length $\tau = f(T)$, where $T = t_{\text{next}} - t_{\text{last}}$ is the recovery time of the cell. If the pulse arrives within the refractory period of the neighbouring cell, the pulse is blocked and does not affect the value of t_{next} of that cell. Otherwise the value of t_{next} is replaced by a new one only if such replacement results in keeping the arrival time of the earliest arriving pulse after the refractory period. Finally t_{last} and t_{next} of the exciting

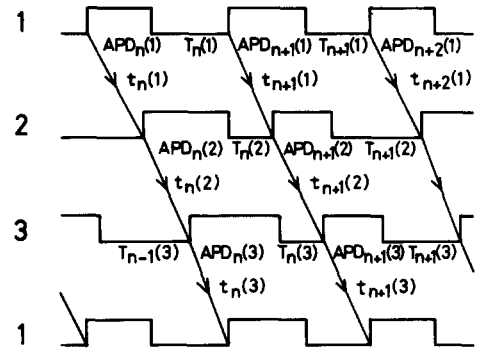

Fig. 3. A schematic view of the uni-directional circulation of excitation pulse in a ring of three cells ($N = 3$). The states of the three cells are shown by three time traces. The trace of cell 1 shown at the top is repeated at the bottom. The cell stays in the excited state (during the action potential) during the elevated base line in the trace and stays in the recovering state between the action potentials. The propagation of the excitation which induces the action potential in the neighbouring cell is shown by a line with arrow showing the direction of conduction.

cell are replaced by $t + \mathrm{APD}$ and ∞, respectively, where $\mathrm{APD} = g(T)$. In the following discussion, we assume there are N cells separated by a distance $l = L/N$, where L is the total length of the ring. The effect of inhomogeneity in the cell spacing will be discussed in section 5.

2.2. *Uni-directional circulation*

This system supports a uni-directional circulation of excitation pulse over the ring for some parameters. Fig. 3 schematically depicts the successive activations of cells following the uni-directional circulation of the excitation in the case of $N = 3$. We define the direction of circulation in fig. 3 clockwise. Although we consider the clockwise circulation, the following discussions apply to the counterclockwise circulation also. In the nth revolution of the excitation over the ring, when the ith cell gets excited, the cell has an action potential with a duration $\mathrm{APD}_n(i)$ and emits an excitation pulse which travels to the $(i+1)$st cell with the conduction time $t_n(i)$. We assume that the excitation conducting to the $(i-1)$st cell is always blocked by the refractory duration of that cell. Every time the excitation pulse returns back to the first cell, the number of revolutions is increased by one. The cycle length between the nth and $(n+1)$st excitations is divided into $\mathrm{APD}_n(i)$ and the recovery time of the cell, $T_n(i)$. The cycle length is also given by the summation of the conduction times for each cell along the ring,

$$\mathrm{APD}_n(i) + T_n(i) = \sum_{j=1}^{i-1} t_{n+1}(j) + \sum_{j=i}^{N} t_n(j), \quad i = 1, \ldots, N. \tag{3}$$

Since $t_{n+1}(i) = lf\{T_n(i)\}$ and $\mathrm{APD}_n(i) = g\{T_{n-1}(i)\}$,

$$T_n(i) = l\left(\sum_{j=1}^{i-1} f\{T_n(j)\} + \sum_{j=i}^{N} f\{T_{n-1}(j)\}\right) - g\{T_{n-1}(i)\}, \quad i = 1, \ldots, N. \tag{4}$$

The N-dimensional map given by eq. (4) transforms $\{T_{n-1}(i)\}$ into $\{T_n(i)\}$. As long as we consider the uni-directional circulation of the excitation pulse, the basic model can be reduced to this N-dimensional map. The map in eq. (4) has a term that represents the global coupling among all the cells on the ring, in addition to the second term that depends only on the local variable $T_n(i)$.

3. Stability analysis

In this section and the next section, we study dynamics in the map given by eq. (4). It is convenient to assume a set of parameters and discuss the dynamical properties by using this example. However our discussion will be focused on the global features of dynamics. The estimation of the actual parameters in real cardiac tissue will be carried out in section 6 where we apply our model to reproduce the experimental data. Based on these results, here we assume the parameters: $N = 8$, $L = 80$ mm, $\gamma = 3$ ms/mm, $\varepsilon = 50$ ms, $\zeta = 220$ ms, and $\theta = 60$ ms.

The fixed point solution $\{T_n(i) = T_0\}$,

$$T_0 = lNf(T_0) - g(T_0), \tag{5}$$

corresponds to the stationary circulation of the excitation pulse with a constant velocity. Fig. 4a shows the phase diagram of the fixed point solution as a function of α and β. We fixed the restitution curve with $\delta = 500$ msec and examined the stability of uni-directional stationary circulation to changes in the recovery curve. The change in the structure of the phase diagram with different δ will be discussed in appendix A. Here we selected a value of δ to show a typical case reflecting the dynamics in the experimental system [9, 36]. In fig. 4b, on the other hand, we fixed $\beta = 30$ ms based on the experimental value estimated in section 6 and examined the stability with different α and δ. In both figures, a hatched region represents the stable region for the fixed point. There are three criteria that must be satisfied in order for the fixed point solution to represent a stable circulating pulse. The stable region is determined by the following three boundaries:

(1) *Reentry (dashed lines in figs. 4b (inset)).* The steady state recovery time T_0 must be greater than the refractory time so that

$$T_0 \geq \theta. \tag{6}$$

This condition is satisfied above the boundary. In fig. 4a, this condition is satisfied over the entire range since θ is small. Explicit forms of this boundary and the other two boundaries can be obtained analytically and are given in appendix A.

(2) *Uni-directional circulation (dot-dashed lines in fig. 4a).* The excitation pulse must be blocked by the refractory duration in the direction opposite to its propagation direction so that

$$2lf(T_0) - g(T_0) < \theta, \tag{7}$$

where $lf(T_0)$ is the conduction time between the

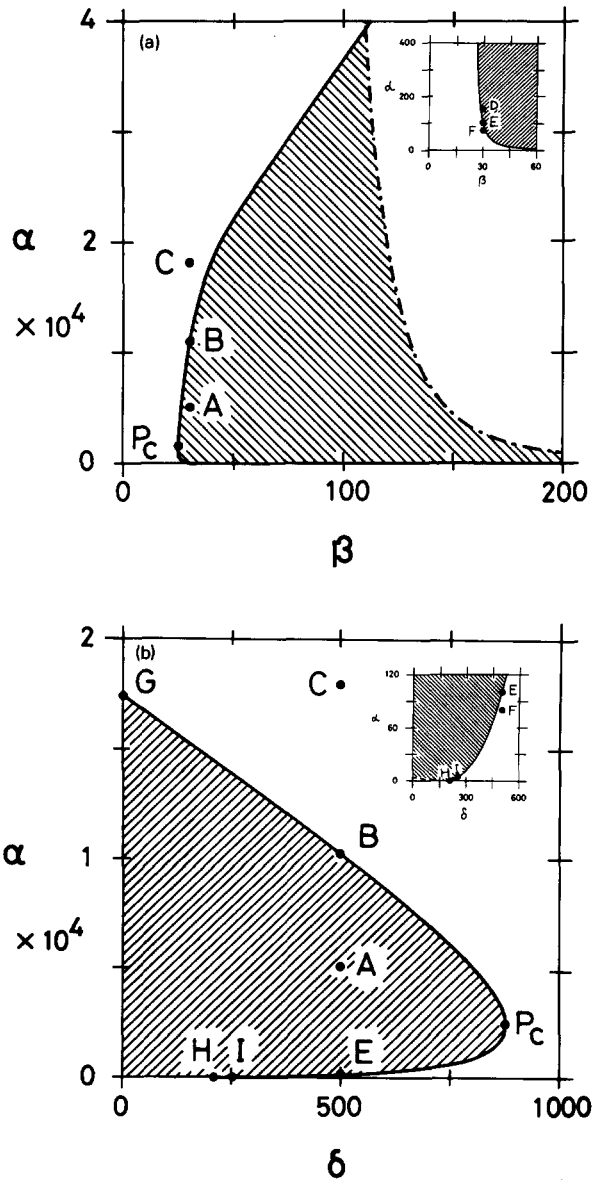

Fig. 4. Phase diagram of the fixed point solution: (a) in (α, β)-space with $\delta = 500$ ms; (b) in (α, δ)-space with $\beta = 30$ ms. $N = 8$, $L = 80$ mm, $\gamma = 3$ ms/mm, $\varepsilon = 50$ ms, $\zeta = 220$ ms, and $\theta = 60$ ms. The units of α, β, and δ are ms/mm, ms, and ms, respectively. In each figure, the inset shows the magnified view of the region of small α. The stable region of the fixed point is shown by a hatching in each figure, which is determined by three independent boundaries: reentry (dashed line), uni-directionality (dot-dashed line), and linear stability (solid line). The points A, B, C, ..., I represent the sets of parameters used for numerical simulations in section 4. P_c is the turning point of the stability boundary where the upper branch and the lower branch meet.

neighbouring cells and $g(T_0)$ is the APD during stationary circulation. This condition is satisfied below the boundary. In fig. 4b, the boundary does not appear, because it is located in the region of very large δ and α for the value of β here. The condition (7) is satisfied over the entire parameter space in fig. 4b.

(3) *Linear stability (solid lines in figs. 4a and 4b).* The linearization of the N-dimensional map (4) around the fixed point gives

$$x_{n+1}(i) = a\left(\sum_{j=1}^{i-1} x_{n+1}(j) + \sum_{j=i}^{N} x_n(j)\right) - cx_n(i),$$

$$i = 1, \ldots, N, \tag{8}$$

where $x_n(i) = T_n(i) - T_0$ is the deviation of $T_n(i)$ away from its steady state value,

$$a = l\frac{\mathrm{d}f}{\mathrm{d}T}\bigg|_{T=T_0}, \tag{9}$$

and

$$c = \frac{\mathrm{d}g}{\mathrm{d}T}\bigg|_{T=T_0}. \tag{10}$$

The stability analysis of eq. (8) shows that N eigenvalues of the stability matrix are within the unit circle in the complex plane and the fixed point is a stable attractor provided

$$a - c > -1. \tag{11}$$

This condition is satisfied on the right side of the boundary in fig. 4a and the left side of the boundary in fig. 4b. At the bifurcation point where $a - c = -1$, N eigenvalues lie on the unit circle in the complex plane and are given by $e^{i\phi}$, where $\phi = \pm\phi_1, \pm\phi_2, \ldots, \pm\phi_{N/2}$, if N is an even integer, and $\phi = \pm\phi_1, \pm\phi_2, \ldots, \pm\phi_{(N-1)/2}, \phi_{(N+1)/2} = \pi$, if N is odd (see proof in appendix B). Therefore the fixed point loses its stability by the degenerate multiple Hopf bifurcation [37–39] in which there is the simultaneous appearance of $N/2$ different oscillation frequencies ($(N+1)/2$, if N is odd) determined by the phases $\{\phi_i\}$. As we change the parameter moving along the stability boundary, the phases $\{\phi_i\}$ vary continuously. Therefore, except for some special cases that have a zero measure in the parameter space, the oscillation frequencies are incommensurate with each other and the neutrally stable oscillations at the bifurcation point are quasiperiodic oscillations with many incommensurate frequencies. In the case when these frequencies are commensurate to each other, we cannot apply the Hopf bifurcation theorem because of the resonance problem [37–39]. These theoretical results are confirmed by numerical simulations in the next section. Furthermore the Hopf bifurcation can be either subcritical or supercritical depending on the parameters. Numerical simulations show that the bifurcation is subcritical on the upper branch of the stability boundary which is above the turning point P_c in figs. 4a and 4b, and supercritical on the lower branch.

4. Dynamics

The results in the previous section help in the study of the dynamics in parameter space. There are four different types of dynamics present in this system: (1) stable circulation with constant cycle length, (2) unstable circulation with divergent oscillation of the recovery time leading to spontaneous termination of reentry, (3) unstable circulation leading to bounded quasiperiodic oscillation of the cycle length, (4) neutrally stable quasiperiodic oscillation at the bifurcation point. As the parameters vary, these different behaviours can be found in the following numerical simulations accompanying characteristic bifurcations. In order to illustrate these different behaviours, we consider a typical subcritical bifurcation in subsection 4.1 and a supercritical bifurcation in subsection 4.2. In the following discussion, we will omit the units of parameters for simplicity.

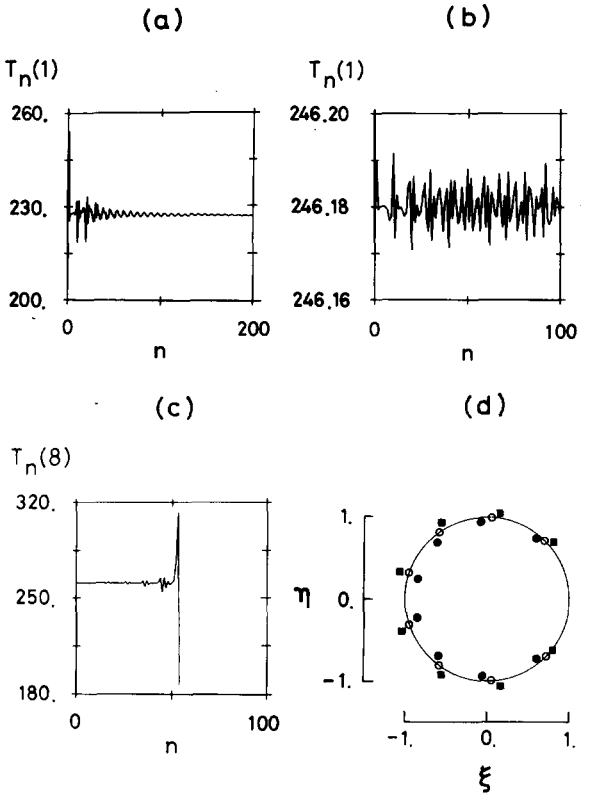

Fig. 5. Response of the N-dimensional map to a small perturbation added to the fixed point with $N = 8$, $\beta = 30$, $\delta = 500$. (a) Plot of recovery time at the first cell, $T_n(1)$, as a function of beat number, n. $\alpha = 5000$, which falls at point A in figs. 4a, 4b. The steady state recovery time $T_0 = 227.67$. (b) Plot of $T_n(1)$ with $\alpha = 10190.13$, point B (bifurcation point). $T_0 = 246.18$. (c) Plot of recovery time at the eighth cell $T_n(8)$ with $\alpha = 18000$, point C. $T_0 = 261.18$. The simulation starts from the initial condition at $n = 0$: every cell has the recovery time T_0 except for the first cell, which has the perturbed recovery time, $T_0 - 20$ (a); $T_0 - 0.01$ (b); $T_0 - 0.2$ (c). (d) Distribution of eigenvalues of the stability matrix given by eq. (8) in the complex plane with $\alpha = 5000$ (closed circles); $\alpha = 10190.13$ (open circles); $\alpha = 18000$ (closed squares). ξ and η are the real part and the imaginary part of the complex number, respectively. The fixed point is linearly stable when all eigenvalues are within the unit circle.

4.1. Subcritical bifurcation on the upper branch of the stability boundary

Figs. 5a–5c show the response of the N-dimensional map to a small perturbation added to the fixed point. In every simulation, $\beta = 30$ and $\delta = 500$. The parameter α in fig. 5a is 5000 which falls at point A in figs. 4a, 4b. The recovery time of the first cell, $T_n(1)$, which is plotted as a function of beat numbers, converges to the stationary value T_0 accompanying a damped oscillation. In fig. 5d, closed circles represent the eigenvalues of the stability matrix in eq. (8) with $a = -0.843$ and $c = 0.105$ calculated from eqs. (9) and (10). Since $a - c = -0.949 > -1$ and every eigenvalue is within the unit circle in the complex plane, the fixed point (stationary circulation) is stable. The bifurcation occurs at the point B in figs. 4a, 4b with $\alpha = 10190.13$ ($a = -0.927$ and $c = 0.073$).

When α is increased above the linear stability boundary with $\alpha = 18000$ which falls at point C in figs. 4a, 4b, every eigenvalue crosses the unit circle (closed squares in fig. 5d where $a - c = -1.048$ with $a = -0.994$ and $c = 0.054$) and the small perturbation to the fixed point grows divergently (fig. 5c). Fig. 5c shows the evolution of the recovery time at the eighth cell, $T_n(8)$. In general the amplitude of the unstable oscillation in the recovery time grows at each cell until the uni-directional circulation is terminated by either of two causes. First, the circulation is terminated when the recovery time becomes less than the refractory time at one of the cells in the ring. The other possibility is the violation of the condition for uni-directional circulation when $t_n(i) + t_n(i+1) - \mathrm{APD}_n(i) > \theta$. In this case, the excitation pulse from the $(i+1)$st cell can excite the ith cell again (excitation echo). In the simulation of fig. 5c, the seventh cell gets excited by the eighth cell because the very short recovery time at the eighth cell results in very slow conduction of excitation pulse. When the condition for uni-directional circulation was violated and the dynamics cannot be described by the N-dimensional map, we stopped the numerical simulation. Although excitation echoes [35] are also interesting, we restrict our study only to uni-directional circulation in this paper.

In the above case, the bifurcation is subcritical. We simulated the map in eq. (4) ignoring both the reentry condition and the uni-directionality condition to see where the divergent oscillation is

attracted. After the fixed point loses its stability, the trajectory is attracted by a period $N+1$ oscillation with very large amplitude. The oscillations in the recovery time take both very small values ($\sim 20 = L\gamma - \zeta$) and very large values ($\sim 10^5$) both of which are outside the normal physiological value. Since the bifurcation is subcritical, even within the stable region in the phase diagram, the basin of attraction of the fixed point is limited in the phase space. Especially near the bifurcation point, most initial conditions are attracted by the large amplitude oscillation accompanying the divergent oscillation until the uni-directional circulation is terminated. Therefore even when the stationary reentry is stable, it may be very difficult to initiate it.

4.2. *Supercritical bifurcation on the lower branch of the stability boundary*

Interestingly, by decreasing α in the stable region in figs. 4a, 4b with $\beta = 30$, we cross the lower branch of the stability boundary and the fixed point loses its stability again. Figs. 6a–6c show the response of the system to the perturbation added to the fixed point with different α. The bifurcation occurs at the point E in figs. 4a, 4b with $\alpha = 100.73$ ($a = -0.351$ and $c = 0.649$). A dominant difference from the bifurcation on the upper branch is that now the bifurcation is supercritical. Therefore, when α is decreased below the stability boundary until $\alpha = 80$ (point F in figs. 4a, 4b), the unstable oscillation around the fixed point is stabilized by nonlinearity and we get the bounded oscillation appearing in fig. 6c. As α is decreased further, the amplitude of the bounded oscillation grows. Finally the recovery time becomes less than the refractory time so that the bounded oscillation can no longer be sustained.

4.3. *Changes of oscillation pattern*

In the above studies, we found different behaviours appearing via characteristic bifurcations.

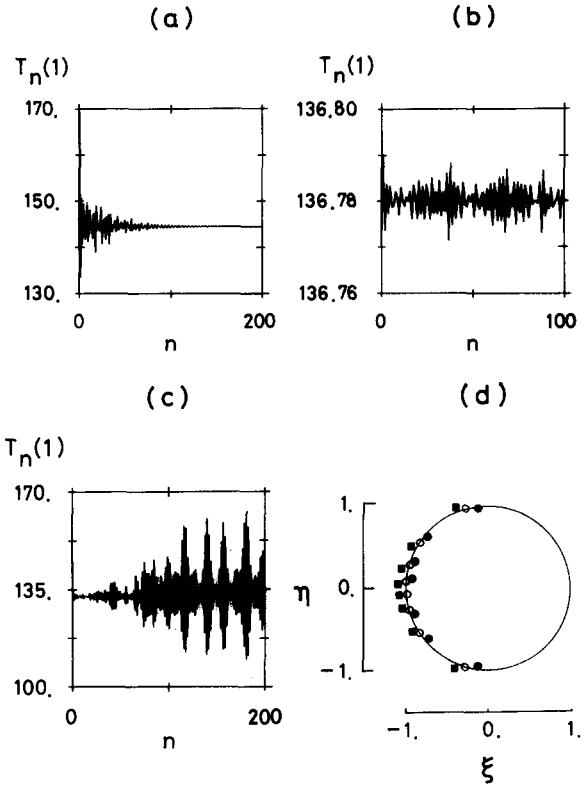

Fig. 6. Plot of $T_n(1)$ with $N = 8$, $\beta = 30$, $\delta = 500$. (a) $\alpha = 150$, point D in figs. 4a, 4b. $T_0 = 144.59$. (b) $\alpha = 100.73$, point E (bifurcation point), $T_0 = 136.78$. (c) $\alpha = 80$, point F, $T_0 = 132.52$. The simulation starts from the initial condition at $n = 0$: every cell has the recovery time T_0 except for the first cell, which has the perturbed recovery time, $T_0 - 20$ (a); $T_0 - 0.01$ (b); $T_0 - 2$ (c). (d) Distribution of eigenvalues of the stability matrix with $\alpha = 150$ (closed circles, $a = -0.404$, $c = 0.555$); $\alpha = 100.73$ (open circles, $a = -0.351$, $c = 0.649$); $\alpha = 80$ (closed squares, $a = -0.322$, $c = 0.706$).

Now we consider another important property of the dynamics. In actual experiments with a ring of cardiac tissue, Frame and Simson observed that different patterns of oscillation in the cycle length are found in different samples of tissue reflecting differences in recovery and restitution curves. Therefore it is important to examine how the oscillation pattern is affected by changes in both characteristic curves.

At first we consider the two limiting cases. When APD is a constant ($\delta = 0$), the second term in eq. (4) is just a constant and the N-dimensional

map has only the dynamics which couples all the cells. The gradient of the restitution curve at the steady recovery time, c, is 0. At the bifurcation point (point G in fig. 4b), the eigenvalues are distributed on the unit circle with equal spacing and every frequency is a harmonic of the fundamental (see appendix B). The neutrally stable oscillation in the recovery time is regular with period $N+1$ and the bifurcation is subcritical. Thus, we cannot obtain the complex oscillation shown in fig. 1 with a constant restitution curve. On the other hand, when $\alpha = 0$, the conduction time does not depend on the recovery time and the first term in eq. (4) is now constant. The N-dimensional map is decoupled into N independent one-dimensional maps. At $c = 1$ (point H in fig. 4b), N identical eigenvalues cross the unit circle at -1 (appendix B). The stationary circulation becomes unstable to a supercritical period doubling bifurcation and the neutrally stable oscillation is regular with period 2.

In general, the bifurcation occurs at some point between the two limiting cases on the stability boundary in fig. 4b and $0 < c < 1$. When there is a change in the parameters as one moves along the stability boundary, the distribution of eigenvalues on the unit circle varies continuously accompanying the change in oscillation profile of the quasiperiodic neutrally stable oscillation (see examples, fig. 5b and 5d: $c = 0.073$ at point B and fig. 6b and 6d: $c = 0.649$ at point E). For example, at another bifurcation point with $\alpha = 3.80$, $\delta = 250$ and $\beta = 30$, point I in fig. 4b, the restitution curve has a very steep slope at the steady recovery time ($c = 0.924$). This results in a close distribution of the phases $\{\phi_i\}$ around π and the neutrally stable oscillation shows alternation of long and short intervals with a characteristic beating pattern (figure not shown).

In summary, in order to obtain the complex oscillations in the period of reentrant circulation observed experimentally, both the recovery curve and the restitution curve are needed and the pattern of oscillation strongly depends on the slope of the restitution curve.

5. Extension to inhomogeneous systems

In the previous sections, we assumed an equal spacing between the cells on the ring. Because of this symmetric arrangement of cells, N eigenvalues of the stability matrix cross the unit circle in the complex plane simultaneously. We performed numerical simulations to determine how the bifurcations in the homogeneous system are modified by inhomogeneities in the cell spacing.

In the ring of N identical cells, the distance between the neighbouring cells is Gaussian distributed around the mean spacing L/N in a random way. We fix the total ring size L so that the steady state recovery time of the stationary circulation T_0 given by eq. (5) is the same as in the homogeneous system, and we assume the same parameters used in sections 4.1 and 4.2. We studied the bifurcations as a function of α. We also examined the system with different degrees of inhomogeneity by changing the standard deviation of the Gaussian distribution in a range of $0 \sim 50\%$ of the mean cell spacing.

First we discuss the bifurcation on the upper branch of the stability boundary in fig. 4b. As discussed in section 4.1, subcritical multiple Hopf bifurcation occurs at point B in fig. 4b with $\alpha = \alpha_c$ ($= 10190.13$) in the homogeneous system. In the inhomogeneous system, by increasing α above the range in which the fixed point is stable, complex conjugate pairs of eigenvalues successively cross the unit circle with different α taking the value $e^{\pm i\phi}$ ($\phi < \pi$). Numerical simulation showed that the pair of eigenvalues with smaller ϕ (unstable mode with a lower frequency) cross the unit circle with smaller α. This property is found in every simulation discussed here. The bifurcation is characterized by three values of α ($\alpha_1, \alpha_2, \alpha_3$). At $\alpha = \alpha_1$ ($< \alpha_c$) the first pair of eigenvalues crosses the unit circle and the fixed point becomes unstable via a *supercritical* Hopf bifurcation. The final pair of eigenvalues crosses the unit circle at α_3 ($> \alpha_c$). For $\alpha > \alpha_3$, all the eigenvalues are outside of the unit circle. In the range where α is slightly greater than α_1, there exists a stable small

amplitude oscillation with a single frequency component reflecting the unique unstable oscillation mode around the fixed point. However as we keep increasing α, the amplitude of bounded oscillation grows and the oscillation begins to contain other frequency components even before the other pairs of eigenvalues cross the unit circle. This appears to reflect nonlinear couplings to other linear modes. However the bounded quasiperiodic oscillation disappears suddenly at a certain value α_2 ($<\alpha_3$). As in the case of the homogeneous cell spacing, the large amplitude oscillation with a period $N+1$ discussed in section 4.1 coexists with the fixed point in the range $\alpha<\alpha_1$ and with the small amplitude bounded oscillation in the range $\alpha_1<\alpha<\alpha_2$. In the range $\alpha>\alpha_2$, every initial point is attracted by a large amplitude oscillation and the uni-directional circulation is terminated by the violation of the uni-directional condition that is the analogue of eq. (7) in inhomogeneous systems.

As we decrease the degree of inhomogeneity in the cell spacing by reducing the standard deviation of the Gaussian distribution, the interval between α_1 and α_3 becomes smaller, and it is finally zero in the homogeneous case ($\alpha_1=\alpha_3=\alpha_c$). Since $\alpha_2<\alpha_3$, the parameter range where the bounded oscillation exists becomes smaller also. In the homogeneous case, there is no parameter range for the bounded oscillation and the bifurcation is the subcritical multiple Hopf bifurcation.

In a similar fashion, on the lower branch of the stability boundary in fig. 4b, the inhomogeneity in the cell spacing leads to successive supercritical Hopf bifurcations associated with successive crossings of the unit circle by pairs of eigenvalues with different α. Since the multiple Hopf bifurcation is supercritical in the homogeneous case, we still observe similar behaviour even in the inhomogeneous system and get bounded quasiperiodic oscillation. Figure 7a shows the stable oscillation that appeared via the Hopf bifurcation. With this α, only one pair of eigenvalues are outside of the unit circle (fig. 7b) that contributes

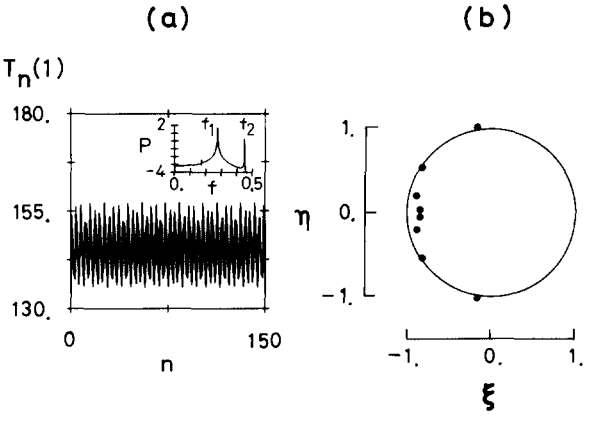

Fig. 7. The stable quasiperiodic oscillation in the system with the inhomogeneous cell spacing. $\alpha=150$ and the standard deviation of the Gaussian distribution for cell spacing is 50% of the mean cell spacing. The other parameters are the same as the simulation in Section 4.2. (a) the oscillation in the recovery time $T_n(1)$ after the system is attracted by the stable oscillation. The inset shows the power spectrum of the stable oscillation computed by 1024 data points. The oscillation mode $e^{i\phi n}$ is characterized by the angular frequency ϕ. The power P in the ordinate is in a logarithmic scale and the abscissa shows $f=\phi/2\pi$. The oscillation has two fundamental frequencies f_1 and f_2. (b) Distribution of eigenvalues of the stability matrix in the complex plane. There is only single pair of eigenvalues outside of the unit circle ($|\lambda|=1.024$). The second pair with $|\lambda|=0.986$ is close to the unit circle.

to the main peak f_1 in the power spectrum in fig. 7a (inset). However there is another frequency component f_2 in the spectrum that we attribute to the second pair of eigenvalues close to the unit circle. The nonlinear coupling between the linear modes leads to a quasiperiodic oscillation similar to that found in the homogeneous case even when there is unique unstable oscillation mode around the fixed point[#1]. These cases on the lower branch are most important physiologically,

[#1] In order to analyze the successive Hopf bifurcation more correctly, we would need to examine the Floquet exponents around the stable oscillation rather than the linear stability around the fixed point [37, 51]. The appearance of the second oscillation mode by the nonlinear coupling between the linear modes was studied in the problem of optical bistability both experimentally and theoretically by using delay differential equations [40, 41].

since the slope of the actual restitution curve observed experimentally is $c = 0.57$–0.95 [19] and this suggests the actual bifurcation should be on the lower branch of the stability boundary.

6. Application to reentrant tachycardias

In the previous sections, we discussed the circulation of an excitation pulse on an excitable ring using the theoretical model. We now apply these results to analyze dynamics in the experimental data from which fig. 1 is derived. In what follows, we simulate the various oscillating behaviours by incorporating the recovery curve and restitution curve reported in the paper by Frame and Simson [19]. We compare the results with the experimental data.

In the previous sections, we assumed that the restitution curve is an exponential function given by eq. (2), since most experimental studies have described the restitution curve as either a single exponential function or a sum of two exponential functions [9, 32, 36]. However Frame and Simson reported that the restitution curve in their experiment was well fitted by a linear relation. They attributed the linearity to the limited ranges of the recovery time (diastolic interval) observed during the oscillation. Therefore in order to compare the results of our simulation with the Frame and Simson experimental data, we assume a linear restitution curve,

$$g(T) = cT + d, \quad \text{if } T \geq \theta, \tag{12}$$

where the parameters c and d are positive. We still assume the nonlinear recovery curve given in eq. (1). We also assume the equal spacing between the neighbouring cells in every simulation in this section. The stability criteria of the unidirectional circulation discussed in section 3 apply to this system also. However, compared with the phase diagram with nonlinear restitution curves shown in figs. 4a, 4b, the stability boundary with linear restitution curves is a single valued as a function of β (in (α, β)-space) and c (in (α, c)-space) and the Hopf bifurcation is always subcritical. When the fixed point loses its stability, the recovery time at each cell oscillates with divergent amplitude until uni-directional circulation is terminated by violation of either the reentry condition or the uni-directionality condition. We do not obtain bounded oscillation with the linear restitution curve in a homogeneous system.

6.1. Resetting stable tachycardias

As Frame and Simson pointed out, although the stable tachycardias do not oscillate spontaneously, they show damped oscillation in cycle length after premature stimuli that reset the tachycardia. Fig. 8 shows the result of numerical simulation of stable tachycardia. In every simulation in this section, we use the original basic model introduced in section 2.1. We assumed the nonlinear recovery curve in eq. (1) and the linear

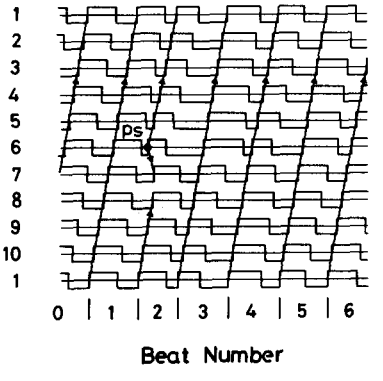

Fig. 8. Resetting of stable tachycardia by a premature stimulus in the basic model with $N = 10$, $\alpha = 4.2$ ms/mm, $\beta = 30$ ms, $\gamma = 3.4$ ms/mm, $c = 0.66$, $d = 78$ msec, and $\theta = 30$ ms. The state of ten cells are shown by ten time traces, where the cell stays in the excited state during the elevated base line and stays in the recovering state between the action potentials (during lowered base line). The beat number, n, is shown at the bottom for first six circulations. Two cycles of stable tachycardia (cycle length 262.7 ms) are shown before the premature stimulus added at cell 6 when cell 6 has recovery time 33 ms (represented by PS in figure).

restitution relation in eq. (12). The parameters are $N = 10$, $\alpha = 4.2$ ms/mm, $\beta = 30$ msec, $\gamma = 3.4$ ms/mm, $c = 0.66$, $d = 78$ ms and $\theta = 30$ ms which were estimated from the data in fig. 1 and fig. 2 in ref. [19]. In the experiment, ten electrodes were equally spaced on a circle around the ring preparation to record the activation at multiple sites. Since they reported the interelectrode distance was 7–8 mm, we assume a ring size $L = 75$ mm. Although the ring size varies in different samples, we always use this value in the following numerical simulations. The problem associated with determining the number of cells, N, will be discussed in the next section. The fixed point solution may be either stable or unstable with different N. Here, we choose a value of N to realize the stable tachycardia.

With these parameters, the stationary circulation of the excitation pulse has a steady cycle length of 262.7 ms which is composed of the recovery time (*diastolic interval*) $T_0 = 111.3$ ms and APD = 151.4 ms. Since a in eq. (9) is -0.026 and $a - c = -0.69 > -1$, the stationary circulation is linearly stable. In fig. 8, initially the excitation pulse showed the stationary counterclockwise circulation on the ring. When the recovery time of cell 6 was 33 msec, we added a premature stimulus to that cell (indicated by PS in fig. 8) which induced the action potential and two excitation pulses conducting towards cell 5 and cell 7 (retrograde conduction). The premature stimulus was added so early that the conducting pulse to cell 7 excited that cell before the original stationary circulation arrived there. However these two excitation pulses conducting in the opposite directions were terminated by pair annihilation, and as a result the tachycardia was reset to create a new circulation pulse. Fig. 8 shows good agreement with the experimental data shown in fig. 1 in ref. [19].

In figs. 9a–9d, we compare the variations in cycle length at different cells from experiment (left traces) which were taken from data in fig. 1 in ref. [19] and theory (right traces). In these figures, the cycle length is constant at the steady

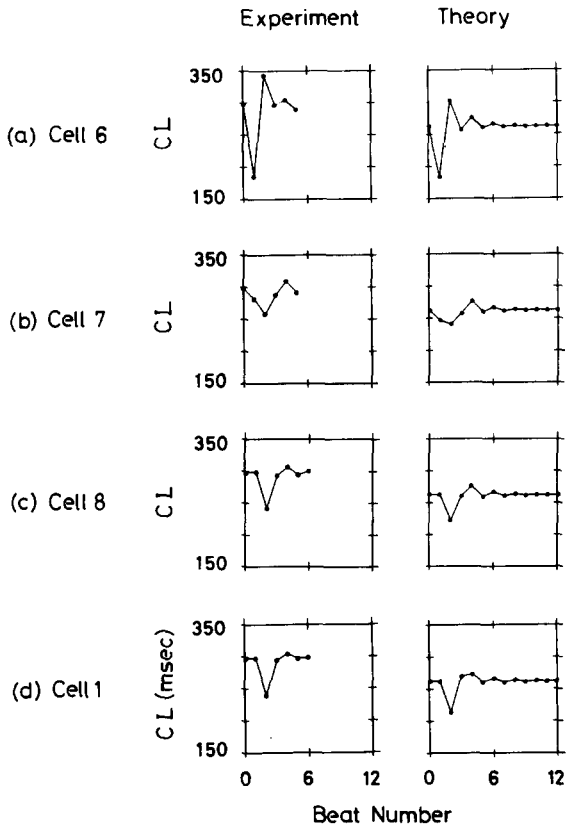

Fig. 9. Cycle length (CL) at different cells in the resetting of the stable tachycardia by premature stimulus: experimental data (left traces, taken from ref. [19]) and numerical simulations (right traces). The CL at (a) cell 6; (b) cell 7; (c) cell 8; (d) cell 1 is plotted as a function of beat number. Since the excitation pulse shows the stationary circulation before the premature stimulus as shown in fig. 8, every cell has the steady state cycle length, 298 ms in the experiment; 263 ms in the simulation. In experimental traces, the data are plotted until the beat number reported in the reference.

state value before the perturbation by the premature stimulation and progressively diminishes in amplitude until the tachycardia returned to its stable steady cycle length. The magnitude of cycle length oscillation and the pattern of oscillation varies at different cells. Our results are in good agreement with the experimental data. We attribute the quantitative disagreement in the steady cycle length between our result (263 ms) and experimental data (298 ms) to the rough estima-

tion of the total ring size and the error in curve fitting of the recovery curve.

6.2. *Unstable tachycardias*

Unstable tachycardias have spontaneous oscillations of cycle length, recovery time, APD and the conduction time. Frame and Simson reported two types of unstable tachycardias: (1) unstable tachycardia with long lasting complex oscillation and (2) unstable tachycardia with divergent oscillation leading to spontaneous termination of reentry. Since both cases are interesting, we reproduce these two behaviours in the following numerical simulations.

6.2.1. *Example 1. quasiperiodic oscillation*

One case showed a rather slow increase in oscillation amplitude and this enabled them to observe the oscillation for a long duration, in fig. 1 in this paper. From their limited data, it is not clear whether this is a stable bounded oscillation or an unstable oscillation with slow increase in its amplitude. Since they reported that the spontaneous oscillation finally terminated the reentry in other recordings from the same sample (fig. 7B in ref. [19]), we assume that the stationary circulation in this sample is unstable but close to the neutrally stable case. In the analysis of the oscillation in fig. 1, although the experimental data showed rather large scatter around their regression line, they applied the linear approximation of the recovery curve in a form

$$\tau = f(T) = a'T + b', \quad \text{if } T \geq \theta, \tag{13}$$

where a' and b' are the parameters which are negative and positive, respectively. In the following simulations, we also assume a linear relation. We estimated $c = 0.90 \sim 0.96$ based on the experimental data in fig. 6 in ref. [19][#2]. This sample has a steeper linear slope in restitution curve than the other samples they reported. The reproduction of the experimental data in fig. 1 was not straightforward because the oscillation pattern (frequency of the beating envelope function) sensitively depends on the parameter c, especially when c is close to 1. Therefore we tried to select the parameters a', b', c and d to best reproduce the oscillation in fig. 1.

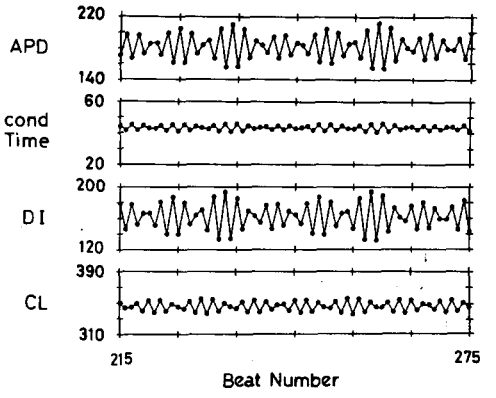

Fig. 10. Spontaneous oscillations during the unstable tachycardia in the theoretical model. The corresponding experimental data are shown in fig. 1. The APD; conduction time of excitation from cell 1 to cell 2; diastolic interval (DI); cycle length (CL) at cell 1 is plotted as a function of beat number, n. The figures show the time domain from $n = 215$ to $n = 275$. The time scales in the ordinates are in ms. $N = 8$, $a' = -0.0086$ mm^{-1}, $b' = 6$ ms/mm, $c = 0.92$, $d = 33$ ms, and $\theta = 100$ ms. The steady state recovery time T_0 is 162.6 ms. We initiated the oscillation by adding a premature stimulus to cell 1 when cell 1 has recovery time 142.4 ms at $n = 1$.

Fig. 10 shows the oscillation in APD, conduction time, recovery time and cycle length. We set the parameters $N = 8$, $a' = -0.0086$ mm^{-1}, $b' = 6$ ms/mm, $c = 0.92$, $d = 33$ ms and $\theta = 100$ ms. The stationary circulation has a cycle length of 345.1 msec with recovery time of 162.6 ms and APD = 182.6 ms. The stationary circulation is unstable because $a = a'l = -0.0806$ and $a - c = -1.0006 < -1$. We selected the parameters to

[#2]They estimated the linear slope in the restitution curve $c = 0.96$ from data in fig. 6C in ref. [19]. However, the slope of the regression line determined from the published figure is approximately 0.90. This small differences does lead to differences in oscillation pattern, see section 4.3.

adjust the frequency of the envelope function in the beating pattern in fig. 1. In order to initiate the oscillation, we perturbed the steady circulation by adding a premature stimulation when the recovery time of cell 1 was 142.4 ms. Comparing fig. 10 with fig. 1, we find that the complex oscillation observed experimentally is a quasiperiodic oscillation.

As Frame and Simson pointed out, the changes in recovery time and APD are much larger than the change in cycle length. In the N-dimensional map in eq. (4), the first term gives the cycle length and the second term gives APD as a function of the previous recovery time at each cell. With the parameters applied in this simulation, the magnitude of the linear slope of the recovery curve ($|a| = 0.0806$) is much less than that of the restitution curve ($c = 0.92$). Therefore the variation in the recovery time leads to a larger variation in APD than that in the cycle length. This always applies to the samples with steep restitution curves.

6.2.2. Example 2. spontaneous termination

Another example of unstable tachycardia was reported in fig. 7A in ref. [19]. We assumed that both recovery and restitution curves are linear and estimated the parameters $a' = -0.071\ \text{mm}^{-1}$, $b' = 19$ ms/mm, $c = 0.57$ and $d = 40$ ms, which were based on their results of linear regression. We assumed $N = 10$ and $\theta = 160$ ms. The cycle length of the stationary circulation is 355.4 ms which is composed of recovery time of 200.9 ms and APD = 154.5 ms. Since $a = a'l = -0.53$ and $a - c = -1.1 < -1$, the stationary circulation is unstable. The unstable oscillation was initiated by adding a premature stimulus at cell 1 with a recovery time 199.5 ms. The uni-directional circulation was terminated at cell 3 after many revolutions because of conduction block by refractoriness. Recovery time at cell 3 is plotted as a function of beat number in fig. 11a as well as the plot of APD, 11b, and cycle length, 11c. The amplitude of each oscillation grows exponentially until the circulation is blocked.

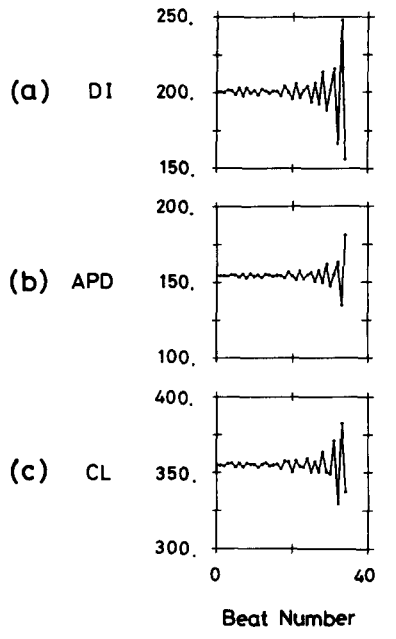

Fig. 11. Spontaneous termination of unstable tachycardia in the theoretical model. Variations in (a) diastolic interval (DI); (b) APD; (c) cycle length (CL) at cell 3, where the conduction block finally occurs, are plotted as a function of beat number. The time scales in the ordinates are in msec. $N = 10$, $a' = -0.071\ \text{mm}^{-1}$, $b' = 19$ ms/mm, $c = 0.57$, $d = 40$ ms, and $\theta = 160$ ms. The steady state recovery time T_0 is 200.9 ms. We initiate the oscillation by adding a premature stimulus to cell 1 when cell 1 has recovery time 199.5 ms.

If we add the premature stimulus at different times, the conduction block may occur at different cells. For example, if we add the stimulus at cell 1 with the recovery time of 199.4 msec, 199.7 ms, 199.9 ms and 200.0 ms, the block happens at cell 2, cell 4, cell 7 and cell 5, respectively. Since the oscillation amplitude of the recovery time grows divergently at each cell and the block occurs at the first cell whose recovery time becomes less than the refractory time, even the slight change of the oscillations causes block in a different cell. Frame and Simson reported that the pattern of the oscillations preceding termination varied considerably among experiments as well as among recordings from the same experiment. Fig. 12 shows the oscillation pattern of the cycle length at the cell where the conduction block occurred

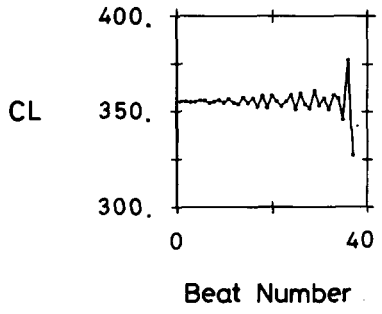

Fig. 12. Cycle length at the cell where the conduction block occurs. The parameters are the same as the simulation in figs. 11a–11c except that we added the premature stimulus at the different time when cell 1 has recovery time 199.9 ms. The conduction block occurs at cell 7.

after the premature stimulus with the recovery time of 199.9 ms. Figs. 11c and 12 show that also in theoretical model the pattern of the oscillation preceding termination varies considerably even in the same system. This example is important since it shows that block does not necessarily occur at some specific location determined by anatomy, but rather at a location determined by the dynamic history.

Since the recovery time at each cell is given by the subtraction of APD from the cycle length, both a long APD and a short cycle length favour a small recovery time which leads to the conduction block. Therefore, although the last recovery time at the site of block is always the smallest, the last cycle length is not necessarily the smallest as seen in fig. 11c. This is also consistent with the experimental observations.

In summary, the theoretical model that incorporates both the experimentally measured recovery and restitution curves is in close quantitative agreement with the dynamics observed in experimental studies of reentrant excitation in a ring of cardiac tissue.

7. Discussion

In this paper we developed a theoretical model for wave conduction in excitable media (coupled maps with continuous time) and applied it to the study of reentrant excitation in the ring of cardiac tissue. The model is based on the recovery curve and the restitution curve of the cardiac tissue. The theoretical model has been analyzed by deriving an analytical stability criteria for the stationary circulation of excitation pulse, and by carrying out numerical simulations incorporating experimentally measured parameters. The simulations give good agreement with experimental data. This is the first theoretical observation of the complex oscillation in the cycle length of reentrant excitation. Moreover the analytical and numerical studies enabled us to reach the following conclusions: (1) A description of wave propagation using low dimensional dynamical systems is not adequate. However, the high dimensional maps give a reasonable approximation to the observed dynamics. (2) Both the recovery curve and the restitution curve of the cardiac tissue are needed to understand the complex oscillations in the cycle length observed experimentally. (3) Oscillations are quasiperiodic and their patterns strongly depend on the slope in the restitution curve at the steady state recovery time. (4) With a nonlinear restitution curve, unstable oscillation may be stabilized and we can get bounded quasiperiodic oscillations over a range of parameters. In the remainder of the discussion, we discuss several different issues raised by this work.

Effect of the nonlinearity in characteristic curves

In section 6, we assumed a linear restitution curve based on experimental data. Since the restitution curves are usually not linear over a broad range of recovery times, further experimental studies of reentrant excitation should be carried out to better characterize the restitution curve. With nonlinear restitution curves, we expect to find a supercritical Hopf bifurcation and bounded quasiperiodic oscillations in the cycle length for some range of parameters. Recently Frame and Rhee [42] studied a system with "adjustable reen-

try" in which the ring was cut and electronically reconnected by sensing activation on one side of the cut and pacing the other side after an adjustable delay. By reducing the delay, they found a bifurcation from a stable stationary circulation to bounded complex oscillations. This phenomenon may correspond to a supercritical Hopf bifurcation with a nonlinear restitution curve.

In the numerical simulation in section 6.2.1, we assumed that the quasiperiodic oscillation in fig. 1 is an unstable oscillation with a slow increase in its amplitude. In fact Frame and Simson observed the spontaneous termination of the reentry by divergent increase in oscillation amplitude in the other recordings from the same sample [19]. However there is a possibility that the data in fig. 1 is a stable quasiperiodic oscillation that coexists with the divergent oscillation attracted by the large amplitude oscillation with a period $N+1$. In section 5, we discussed the coexistence of two attractors on the upper branch of the stability boundary in the inhomogeneous system with the exponential restitution curve. We found such a coexistence over a range of parameters even with the linear restitution curve, if the recovery curve is nonlinear and the cell spacing is inhomogeneous. However we cannot obtain any bounded oscillation when both the recovery curve and the restitution curve are linear as in the simulation in section 6.2.1 even in the inhomogeneous system. Therefore better characterization of the recovery curve is also important to determine the nature of the quasiperiodic oscillation in fig. 1.

Relation to other works

Previous studies of excitation on a ring of tissue were undertaken by Quan and Rudy [43]. They carried out numerical simulations of partial differential equations based on ionic mechanisms and demonstrated the instability of stationary circulation of excitation pulse and the appearance of non-steady oscillation in the APD when they reduced the ring size. However they did not carry out a theoretical analysis of this bifurcation. Their model did not display the oscillation in cycle length observed in the experiment by Frame and Simson [19]. Kopell and Howard also studied the stability of travelling wave solutions on different ring size for general reaction diffusion systems with limit cycle kinetics (oscillatory media) [44, 45].

In this work, we used high dimensional coupled maps to approximate the observed dynamics. Coupled maps were introduced by Kaneko [46, 47] as a mathematical model to study high dimensional chaotic system (coupled map lattice). Coupled maps have been applied to modelling the practical physical systems because of their simple mathematical structure and efficient computational algorithm [48]. Coupled maps with global interaction among all the elements like our model have been attracting attention recently because of their complex properties [49]. We restricted our studies only near the stability boundaries of the fixed point in the phase diagram. It is of great theoretical and experimental interest to study the dynamics of the bounded oscillations far away from the stability boundary. Preliminary numerical simulations suggest the existence of the frequency locking of the high dimensional torus and a quasiperiodic route to chaos [50, 51] over some ranges of parameters.

Mathematical foundation of the model

Because traditional mathematical approach to the studies of the spread of excitation is based on nonlinear partial differential equations, it is important to consider continuum limits of our model. A simple continuum limit of our model can be taken when N goes to infinity keeping the total ring size $L = Nl$ constant. We summarize the change in the phase diagram in appendix A. In this limit, the reentry boundary is independent of N. A single cell is connected with two infinitesimally close neighbouring cells and the conduction time between the two cells is zero. The

uni-directionality condition is trivially satisfied and the recovery curve does not play any role on the instability of the stationary circulation. The instability occurs only via the period doubling bifurcation by the steep restitution curve. Therefore the quasiperiodic oscillation can be observed in our model only with finite N.

A different and more realistic way to approach the continuum limit is to introduce an interaction range of the cell, R. Each cell is connected to all the cells within R and the number of neighbouring cells $\#_{nn} = 2[R/l]$, where $[x]$ represents the maximum integer not exceeding x. The cell receives excitation pulses from these neighbouring cells and becomes excited when the number of incoming pulses after the refractory period exceeds a threshold value N_{th}. The continuum limit can be taken when the number of cells on the ring N goes to infinity keeping $L = Nl$, R, and the ratio $N_{th}/\#_{nn}$ constant. We performed numerical simulations with $L = 80$ mm and $R = 10$ mm to see the behaviour in this continuum limit. The same parameters were assumed for the recovery curve and the restitution curve as in section 4.2. Our original model analyzed in this paper is realized when $N = 8$, $l = 10$ mm, $\#_{nn} = 2$, and $N_{th} = 1$ ($N_{th}/\#_{nn} = 0.5$). As shown in section 4.2, the stationary circulation becomes unstable and the stable quasiperiodic oscillation appears in the cycle length of each cell with $\alpha < \alpha_c = 100.73$ ms/mm. We studied the case with $N = 80$, $l = 1$ mm, $\#_{nn} = 20$, $N_{th} = 10$ ($N_{th}/\#_{nn} = 0.5$). Although the bifurcation occurs with smaller α ($\alpha_c \sim 45$ ms/mm), the stable quasiperiodic oscillation does appear with $\alpha < \alpha_c$. We further increased N to 160 ($l = 0.5$ mm, $\#_{nn} = 40$, $N_{th} = 20$) and obtained almost identical results to the case with $N = 80$. This suggests the system is close to the continuum limit with $N = 80$. Thus, we conclude that our simple model analyzed in this paper captures the essential mechanism leading to the stable quasiperiodic oscillation in the cycle length of the reentrant excitation and the qualitatively similar phenomenon will be preserved even in the continuum limit.

The number of independent aggregates N and the distance between the neighbouring aggregates l in our original model, respectively, correspond to the ratio L/R and the interaction range R in the continuum limit. Since we do not know the interaction range in the actual cardiac tissue, there is an ambiguity in determining the number of independent aggregates N in our theoretical model. When the recovery curve and the restitution curve are given, the steady recovery time of the stationary circulation T_0 is independent of N because eq. (5) does not contain N with fixed $L = lN$. However the stability of the stationary circulation does depend on N through the parameter a in eq. (9). Since $l = L/N$, the stationary circulation may become either stable (i.e., $a - c > -1$) with a large N or unstable with a small N. Therefore we adjusted the parameter N to reproduce the experimental data (stable tachycardia or unstable tachycardia) in the last section. We assumed $l = 7$–9 mm, which is large compared to the space constant $\Lambda \sim 1$ mm in the continuous description of heart muscle [52, 53]. Since the space constant is defined by the response to a subthreshold stimulus (i.e., one that does not induce an action potential), it might not correctly represent the interaction range appropriate for this model of reentrant excitation. Our estimations of the parameter N are supported by the fact that the reproduction of the experimental data was satisfactory and the adjusted N's were consistent for three samples ($N = 8$–10) which have the similar ring size but show different dynamics. The connection between our model and continuous partial differential equations [23, 24, 25] still needs to be investigated.

Our approach should also be applicable to study the spread of excitation in two and three dimensions taking into account realistic properties of complex excitable media. Recent experiments [54, 55] and numerical simulations of theoretical models [56, 57] have suggested that, in continuous excitable (chemical) media, the instability of stationary rotating spiral waves to meandering motion arises via a Hopf bifurcation. It is

a challenging problem to study this transition using our theoretical model.

Acknowledgements

We thank M.R. Guevara and J. Bélair for helpful conversations. This research is supported by grants from the Natural Science and Engineering Research Council of Canada, the Heart and Stroke Foundation of Quebec, and les Fonds des Recherches en Santé du Québec. H.I. is a research fellowship of the Heart and Stroke Foundation of Canada.

Appendix A. Forms of boundaries

As discussed in section 3, the stable region for the fixed point solution of the map in eq. (4) is determined by three independent boundaries in the phase diagram (figs. 4a and 4b). In this appendix we show their explicit analytical forms. The three boundaries are obtained by imposing the equality between the r.h.s. and l.h.s. in the conditions given in eqs. (6), (7) and (11).

(1) Reentry. Substituting the expressions of $f(T_0)$ and $g(T_0)$ given by eqs. (1) and (2), respectively, into eq. (5) and assuming $T_0 = \theta$ in eq. (6), we obtain

$$\alpha s = (\theta - L\gamma + \zeta - \delta e^{-\theta/\varepsilon}) e^{\theta/\beta}/L, \qquad (A.1)$$

which determines the boundaries in (α, β)-space and (α, δ)-space.

(2) Uni-directional circulation. Eq. (5) and $2lf(T_0) - g(T_0) = \theta$ in eq. (7) give the relations

$$\alpha = (\theta - 2l\gamma + \zeta - \delta e^{-T_0/\varepsilon}) e^{T_0/\beta}/2l, \qquad (A.2)$$

and

$$T_0 = [N\theta + (N-2)(\zeta - \delta e^{-T_0/\varepsilon})]/2. \qquad (A.3)$$

The boundaries in figs. 4a and 4b were obtained by eq. (A.2) after substituting T_0 which was calculated by solving the transcendental equation (A.3) numerically.

(3) Linear stability. Eq. (5) and $a - c = -1$ in eq. (11) give

$$\alpha = \beta(1 - \delta e^{-T_0/\varepsilon}/\varepsilon) e^{T_0/\beta}/l, \qquad (A.4)$$

and

$$T_0 = \delta(1 - N\beta/\varepsilon) e^{-T_0/\varepsilon} + N\beta + lN\gamma - \zeta. \qquad (A.5)$$

Substitution of T_0 calculated by solving the transcendental equation (A.5) into eq. (A.4) gives the boundaries.

The structure of the linear stability boundary in (α, β)-space depends on δ. Fig. A.1 shows the phase diagram of the fixed point for $\delta = 0$ when the restitution curve is a constant. The other parameters are the same as those in fig. 4a. With δ less than $\delta_0 = \varepsilon \exp\{(L\gamma - \zeta + \varepsilon)/\varepsilon\} \sim 202.76$, the linear stability boundary is a single valued function of β as seen in fig. A.1 and numerical simulations showed that the bifurcation is always

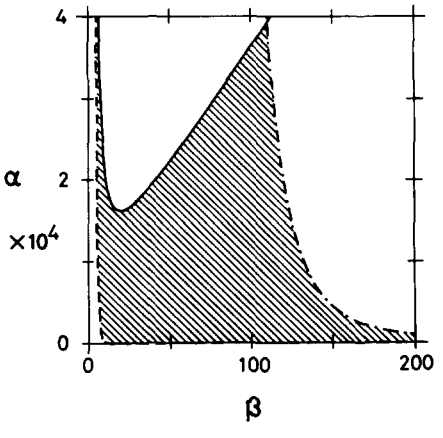

Fig. A.1. Phase diagram of the fixed point solution in (α, β)-space with $\delta = 0$. The other parameters are the same as fig. 4a: $N = 8$, $L = 80$ mm, $\gamma = 3$ ms/mm, $\varepsilon = 50$ ms, $\zeta = 220$ ms, and $\theta = 60$ ms. The units of α and β are ms/mm and msec, respectively. The hatched area shows the stable region of the fixed point which is determined by three independent boundaries: reentry (dashed line), uni-directionality (dot-dashed line) and linear stability (solid line).

subcritical. As δ is increased from zero, the dip in the linear stability boundary moves downwards and the left branch of the dip moves left. At $\delta = \delta_0$, the dip becomes tangential to the β-axis and its left branch is on the α-axis. When $\delta > \delta_0$, the left branch of the dip disappear from the positive β region and the lower branch emerges from the β-axis. The boundary is a two-valued function of β (see fig. 4a). The numerical simulations showed that the bifurcation is subcritical on the upper branch which is above the point P_c in fig. 4a and supercritical on the lower branch. The turning point P_c is at $\beta = \beta_c$ which is given by the transcendental equation

$$\beta_c = \frac{\varepsilon}{N}\left[1 + \frac{\varepsilon}{\delta}\exp\left(\frac{N\beta_c + L\gamma - \zeta}{\varepsilon} - 1\right)\right]. \quad \text{(A.6)}$$

On the other hand, as δ is increased from zero, the reentry boundary in fig. A.1 moves left and finally leaves the positive β region so that the reentry condition is satisfied over the entire (α, β)-space (fig. 4a). In fig. 4b, the linear stability boundary in (α, δ)-space with $\beta = 30$ is also a two-valued function of δ within the range $\delta_0 \leq \delta < \delta_c$, where $\delta_0 \sim 202.76$ and δ at the turning point P_c is $\delta_c = \varepsilon^2 \exp[(N\beta + L\gamma - \zeta - \varepsilon)/\varepsilon]/(N\beta - \varepsilon) \sim 877.45$. The bifurcation is subcritical on the upper branch above the point P_c and supercritical on the lower branch.

In summary, in the experiment of the reentrant excitation on the ring of cardiac tissue, we expect the supercritical Hopf bifurcation of the stationary circulation and the bounded complex oscillations in the cycle length when the sample has a strongly nonlinear restitution curve (large δ).

A simple continuum limit of our model can be taken when N goes to infinity keeping $L = Nl$ constant. Even in this limit, the steady state recovery time T_0 and the reentry boundary given by eq. (A.1) remain the same. On the other hand, the uni-directionality boundary given by eqs. (A.2) and (A.3) goes to $\alpha = \infty$ in (α, β) space (see fig. 4a and fig. A.1) and to $\alpha = \delta = \infty$ in (α, δ) space. In the continuum limit, the uni-directionality condition is trivially satisfied everywhere in the parameter space. With $\delta < \delta_0$, the stability boundary in (α, β) space (fig. A.1) goes to $\alpha = \infty$ and the stationary circulation is stable everywhere in the continuum limit. δ_0 is independent of N. When $\delta > \delta_0$, the turning point of the stability boundary in (α, β) space (point P_c in fig. 4b) goes to $(\alpha, \beta) = (\infty, 0)$ accompanying the movement of the upper branch to $\alpha = \infty$. On the other hand, the lower branch approaches to the monotonically decreasing function of β

$$\alpha = [\varepsilon \ln(\delta/\varepsilon) - \varepsilon - L\gamma + \zeta](\delta/\varepsilon)^{\varepsilon/\beta}/L, \quad \text{(A.7)}$$

that is given by eq. (5) and $c = g'(T_0) = 1$. The stationary circulation is stable above this boundary and the bifurcation is supercritical period doubling everywhere on the boundary. The turning point of the stability boundary in (α, δ) space (point P_c in fig. 4b) goes to $(\alpha, \delta) = (\infty, \infty)$ and the upper branch goes to $\alpha = \delta = \infty$. The lower branch approaches to the boundary given by eq. (A.7) which is a monotonically increasing function of δ starting from the point $(\alpha, \delta) = (0, \delta_0)$. The stationary circulation loses its stability below this boundary via a supercritical period doubling bifurcation.

In this paper, we focused on the local bifurcations around the fixed point. Recent numerical simulations on global structure in phase space suggest a complex structure of the bifurcation diagram. Even in a case of supercritical bifurcation, the large amplitude oscillation with a period $N + 1$ discussed in section 4.1 may coexist with the small amplitude quasiperiodic oscillation over some ranges of parameters. In such a case, initial conditions are attracted either by the small amplitude oscillation or by the large amplitude oscillation until the reentry is terminated. Further, in section 5, we found that inhomogeneity in the cell spacing leads to the coexistence of the two attractors even on the upper branch of the stability boundary.

Appendix B. Calculation of stability eigenvalues

The linear stability of the fixed point in the map (4) can be examined by the eigenvalues of the stability matrix **M** obtained from the linear equation (8). At first, eq. (8) must be transformed into the matrix equation

$$\boldsymbol{x}_{n+1} = \mathbf{M} \cdot \boldsymbol{x}_n, \tag{B.1}$$

where

$$\boldsymbol{x}_n = \begin{pmatrix} x_n(1) \\ \vdots \\ x_n(N) \end{pmatrix}.$$

Because of the symmetry in this system, eq. (8) can be written in a simple form,

$$\boldsymbol{x}_{n+1} = (a-c)\mathbf{I} \cdot \boldsymbol{x}_n + a\mathbf{D} \cdot \boldsymbol{x}_n + a\mathbf{D}^{\mathrm{T}} \cdot \boldsymbol{x}_{n+1}, \tag{B.2}$$

where **I** is the $N \times N$ identity matrix,

$$\mathbf{D} = \begin{pmatrix} 0 & 1 & \dots & 1 \\ 0 & \ddots & \ddots & \vdots \\ \vdots & \ddots & \ddots & 1 \\ 0 & \dots & 0 & 0 \end{pmatrix},$$

and $\mathbf{D}^{\mathrm{T}}$ is the transposed matrix of **D**. The expression in eq. (B.2) is for clockwise circulation of the excitation pulse on the ring as shown in fig. 3. If we consider counterclockwise circulation, we get

$$\boldsymbol{x}_{n+1} = (a-c)\mathbf{I} \cdot \boldsymbol{x}_n + a\mathbf{D}^{\mathrm{T}} \cdot \boldsymbol{x}_n + a\mathbf{D} \cdot \boldsymbol{x}_{n+1},$$

where, in this notation, every time the excitation pulse returns back to the Nth cell, the number of revolutions, n, is increased by one.

From eq. (B.2), we obtain

$$\boldsymbol{x}_{n+1} = (\mathbf{I} - a\mathbf{D}^{\mathrm{T}})^{-1}[(a-c)\mathbf{I} + a\mathbf{D}] \cdot \boldsymbol{x}_n, \tag{B.3}$$

where $\mathbf{A}^{-1}$ represents the inverse matrix of **A**. Comparing eq. (B.3) with eq. (B.1), we get

$$\mathbf{M} = (\mathbf{I} - a\mathbf{D}^{\mathrm{T}})^{-1}[(a-c)\mathbf{I} + a\mathbf{D}]. \tag{B.4}$$

In order to examine the linear stability of eq. (B.2), we have to determine the eigenvalues by solving the equation

$$\mathbf{M} \cdot \boldsymbol{x}_n = \lambda \boldsymbol{x}_n. \tag{B.5}$$

By using eqs. (B.4) and (B.5) and multiplying both side by $\mathbf{I} - a\mathbf{D}^{\mathrm{T}}$ from left, we obtain

$$[(a-c-\lambda)\mathbf{I} + a\mathbf{D} + a\lambda\mathbf{D}^{\mathrm{T}}] \cdot \boldsymbol{x}_n = \mathbf{0}, \tag{B.6}$$

where **0** is the zero column vector. The matrix $\mathbf{A} = (a-c-\lambda)\mathbf{I} + a\mathbf{D} + a\lambda\mathbf{D}^{\mathrm{T}}$ has the form

$$\mathbf{A} = \begin{pmatrix} a-c-\lambda & a & \dots & a \\ a\lambda & \ddots & \ddots & \vdots \\ \vdots & \ddots & \ddots & a \\ a\lambda & \dots & a\lambda & a-c-\lambda \end{pmatrix}.$$

From eq. (B.6), the eigenvalue λ is given by the root of the characteristic equation, $\det(\mathbf{A}) = 0$. Let $\{\boldsymbol{a}_k\}$, $k = 1, \dots, N$, be the row vectors of **A**, i.e.,

$$\mathbf{A} = \begin{pmatrix} \boldsymbol{a}_1 \\ \vdots \\ \boldsymbol{a}_N \end{pmatrix},$$

where

$$\boldsymbol{a}_k = a\lambda \sum_{l=1}^{k-1} \boldsymbol{e}_l + (a-c-\lambda)\boldsymbol{e}_k + a \sum_{l=k+1}^{N} \boldsymbol{e}_l, \quad k = 1, \dots, N, \tag{B.7}$$

and the kth element of the unit row vector $\boldsymbol{e}_k$ is unity and others are zero.

A property of the determinant leads to

$$\begin{aligned} \det(\mathbf{A}) &= \det(\boldsymbol{a}_1, \boldsymbol{a}_2, \dots, \boldsymbol{a}_N) \\ &= \det(\boldsymbol{b}_1 = \boldsymbol{a}_1, \boldsymbol{b}_2 = \boldsymbol{a}_2 - \boldsymbol{a}_1, \dots, \\ &\quad \boldsymbol{b}_N = \boldsymbol{a}_N - \boldsymbol{a}_{N-1}), \end{aligned} \tag{B.8}$$

where

$$\begin{aligned} \boldsymbol{b}_k &= \boldsymbol{a}_k - \boldsymbol{a}_{k-1} \\ &= [(1+a)\lambda - a + c]\boldsymbol{e}_{k-1} - (\lambda + c)\boldsymbol{e}_k, \\ & k = 2, \ldots, N. \end{aligned} \tag{B.9}$$

Finally, using

$$\begin{aligned} &\det(\boldsymbol{b}_1, \ldots, \boldsymbol{b}_N) \\ &= \frac{1}{\lambda - 1} \det((\lambda - 1)\boldsymbol{b}_1, \boldsymbol{b}_2, \ldots, \boldsymbol{b}_N) \\ &= \frac{1}{\lambda - 1} \det\left((\lambda - 1)\boldsymbol{b}_1 - \sum_{l=2}^{N} \boldsymbol{b}_l, \boldsymbol{b}_2, \ldots, \boldsymbol{b}_N\right), \end{aligned} \tag{B.10}$$

and

$$\begin{aligned} &(\lambda - 1)\boldsymbol{b}_1 - \sum_{l=2}^{N} \boldsymbol{b}_l \\ &= -\lambda(\lambda + c)\boldsymbol{e}_1 + [(1+a)\lambda - a + c]\boldsymbol{e}_N, \end{aligned} \tag{B.11}$$

we obtain

$$\begin{aligned} \det(\mathbf{A}) &= \frac{1}{\lambda - 1} \begin{vmatrix} -\lambda p & 0 & \ldots & 0 & q \\ q & -p & \ddots & \ddots & 0 \\ 0 & \ddots & \ddots & \ddots & \vdots \\ \vdots & \ddots & \ddots & \ddots & 0 \\ 0 & \ldots & 0 & q & -p \end{vmatrix} \\ &= \frac{(-1)^N}{(\lambda - 1)} (\lambda p^N - q^N), \end{aligned} \tag{B.12}$$

where $p = \lambda + c$ and $q = (1+a)\lambda - a + c$. Although N eigenvalues are given by the roots of the algebraic equation

$$\begin{aligned} \det(\mathbf{A}) = \frac{(-1)^N}{(\lambda - 1)} \{ &\lambda(\lambda + c)^N \\ &- [(1+a)\lambda - a + c]^N \} = 0, \end{aligned} \tag{B.13}$$

they cannot be solved analytically with general a and c. Therefore, in figs. 5d and 6d, the N eigenvalues were calculated numerically from the matrix **M**.

When $a - c = -1$, the algebraic equation

$$\frac{\lambda(\lambda + c)^N - (c\lambda + 1)^N}{\lambda - 1} = 0, \tag{B.14}$$

becomes a reciprocal equation [58], that is, if $\lambda = \lambda_i$ is a root of this equation, $\lambda = 1/\lambda_i$ is also. Since the complex conjugate of $\lambda_i = r\,e^{i\phi}$, $\bar{\lambda}_i = r\,e^{-i\phi}$ is also a root of the equation and $1/\lambda_i = e^{-i\phi}/r$, r must be unity. Thus we proved that with $a - c = -1$, every eigenvalue of the stability matrix **M** lies on the unit circle in the complex plane. Numerical computations showed that every eigenvalue is within the unit circle when $a - c > -1$ and outside when $a - c < -1$. In summary, at the bifurcation point $a - c = -1$, N eigenvalues of the stability matrix cross the unit circle in the complex plane simultaneously and the fixed point becomes unstable to the appearance of many oscillation modes (degenerate multiple Hopf bifurcation [37–39]).

We can solve the algebraic equation (B.14) in two special cases. First, when the APD does not depend on the recovery time, the slope of the restitution curve c is zero and eq. (B.14) becomes

$$\frac{\lambda^{N+1} - 1}{\lambda - 1} = 0. \tag{B.15}$$

The roots are given by $\lambda_m = z^m$, $m = 1, \ldots, N$, where $z = \exp[2\pi i/(N+1)]$, and are equally spaced on the unit circle in the complex plane. The second special case occurs when the slope of the recovery curve a is zero and the conduction time does not depend on the recovery time. Now $c = 1$ and we get the equation $(\lambda + 1)^N = 0$ whose N roots take the same value -1.

References

[1] L.N. Katz, Electrocardiography (Lea and Febiger, Philadelphia, 1946).

[2] A.G. Mayer, Carnegie Institute. Papers, Washington Tortugas Lab, no. 102 part VII (Carnegie Institute Publication, Washington, 1908) p. 113.

[3] G.R. Mines, Trans. R. Soc. Can. 4 (1914) 43.
[4] T. Lewis and A.M. Master, Heart 12 (1925) 209.
[5] J. Jalife, ed., Mathematical Approaches to Cardiac Arrhythmias, Ann. N.Y. Acad. Sci. 591 (1990).
[6] L. Glass, P. Hunter and A. McCulloch, eds., Theory of Heart, (Springer, New York, 1991).
[7] M.R. Guevara, L. Glass and A. Shrier, Science 214 (1981) 1350.
[8] D.R. Chialvo and J. Jalife, Nature, London 330 (1987) 749.
[9] T. Lewis and M.R. Guevara, J. Theor. Biol. 146 (1990) 407.
[10] M.N. Levy, P.J. Martin, H. Zieske and D. Adler, Circ. Res. 34 (1974) 697.
[11] M.B. Simson, J.F. Spear and E.N. Moore, Am. J. Physiol. 240 (1981) H947.
[12] A. Shrier, H. Dubarsky, M. Rosengarten, M.R. Guevara, S. Nattel and L. Glass, Circulation 76 (1987) 1196.
[13] C.J. Wiggers, Am. Heart J. 20 (1940) 399.
[14] A.T. Winfree, When Time Breaks Down (Princeton Univ. Press, Princeton, 1987).
[15] D.T. Kaplan, The dynamics of cardiac electrical instability, Ph.D. Thesis, (Harvard Univ., Cambridge, 1989).
[16] D.T. Kaplan and R.J. Cohen, Circ. Res. 67 (1990) 886.
[17] A.L. Goldberger and E. Goldberger, Clinical Electrocardiography, 3rd Ed. (The C.V. Mosby, St. Louis, 1986).
[18] R. Yee, G.J. Klein, A.D. Sharma, O. Fujimura, and K.A. Boahene, in: Cardiac Electrophysiology: from Cell to Bedside, eds. D.P. Zipes and J. Jalife (W.B. Saunders, Philadelphia, 1990) p. 463.
[19] L.H. Frame and M.B. Simson, Circulation 78 (1988) 1277.
[20] M.B. Simson, M. Shinner and L.H. Frame, Circulation 78 (1988) II-156, abstract.
[21] L.H. Frame and E.K. Rhee, Circ. Res. 68 (1991) 493.
[22] N. Wiener and A. Rosenblueth, Arch. Inst. Cardiol. Mex. 16 (1946) 205.
[23] A.T. Winfree, SIAM/AMS Proc. 8 (1974) 13.
[24] V.S. Zykov, Simulation of Wave Processes in Excitable Media (Manchester Univ. Press, Manchester, 1987).
[25] J.J. Tyson and J.P. Keener, Physica D 32 (1988) 327.
[26] G.K. Moe, W.C. Rheinboldt and J.A. Abildskov, Am. Heart J. 67 (1964) 200.
[27] J.M. Smith and R.J. Cohen, Proc. Nat. Acad. Sci. USA 81 (1984) 233.
[28] M. Gerhardt, H. Schuster and J.J. Tyson, Science 247 (1990) 1563.
[29] M. Gerhardt, H. Schuster and J.J. Tyson, Physica D 46 (1990) 392.
[30] M. Markus and B. Hess, Nature 347 (1990) 56.
[31] H. Ito and L. Glass, Phys. Rev. Lett. 66 (1991) 671.
[32] M.R. Boyett and B.R. Jewell, J. Physiol. 285 (1978) 359.
[33] R.N. Miller and J. Rinzel, Biophys. J. 34 (1981) 227.
[34] M. Courtemanche and A.T. Winfree, Int. J. Bifurcation Chaos 1 (1991) 431.
[35] V.I. Krinskii, Biophysics 16 (1971) 88.
[36] M.R. Guevara, G. Ward, A. Shrier and L. Glass, in: Computers in Cardiology IEEE Computer Society, (Silver Spring, 1984) p. 167.
[37] J. Guckenheimer and P. Holmes, Nonlinear Oscillations, Dynamical Systems and Bifurcations of Vector Fields (Springer, New York, 1983).
[38] M. Golubitsky and D.G. Schaeffer, Singularities and Groups in Bifurcation Theory, vol. I (Springer, New York, 1985).
[39] M. Golubitsky, I. Stewart and D.G. Shaeffer, Singularities and Groups in Bifurcation Theory, Vol. II (Springer, New York, 1988).
[40] P. Nardone, P. Mandlel, and R. Kapral, Phys. Rev. A 33 (1986) 2465.
[41] R. Vallée and C. Delisle, Phys. Rev. A 34 (1986) 309.
[42] L.H. Frame and E.K. Rhee, Circulation 80 (1989) II-96, abstract.
[43] W. Quan and Y. Rudy, Circ. Res. 66 (1990) 367.
[44] N. Kopell and L.N. Howard, Stud. Appl. Math. 52 (1973) 291.
[45] L.N. Howard and N. Kopell, Stud. Appl. Math. 56 (1977) 95.
[46] K. Kaneko, Prog. Theor. Phys. 72 (1984) 480.
[47] J. Crutchfield and K. Kaneko, in: Directions in Chaos, ed. H.B. Lin (World Scientific, Singapore, 1987).
[48] Y. Oono and A. Shinozaki, Forma 4 (1989) 75.
[49] K. Kaneko, Physica D 41 (1990) 137.
[50] D. Ruelle and F. Takens, Commun. Math. Phys. 20 (1971) 167.
[51] P. Bergé, Y. Pomeau, and C. Vidal, Order within Chaos (Wiley/Hermann, Paris, 1984).
[52] J.P. Keener, in: Theory of Heart, ed. L. Glass, P. Hunter and A. McCulloch, (Springer, New York, 1991) p. 405.
[53] A.T. Winfree, in: Theory of Heart, ed. L. Glass, P. Hunter and A. McCulloch, (Springer, New York, 1991) p. 477.
[54] W. Jahnke, W.E. Skaggs and A.T. Winfree, J. Phys. Chem. 93 (1989) 740.
[55] G.S. Skinner and H.L. Swinney, Physica D 48 (1991) 1.
[56] E. Lugosi, Physica D 40 (1989) 331.
[57] D. Barkley, M. Kness and L.S. Tuckerman, Phys. Rev. A 42 (1990) 2489.
[58] L.E. Dickson, New First Course in the Theory of Equations (Wiley, New York, 1939).